ANNALS OF GEOPHYSICS, 68, 4, V451, 2025; doi:10.4401/ag-9224
OPEN ACCESS

Geometric scaling of felsic sheet intrusions in the brittle upper crust, eastern Elba Island, Italy, with implications for host-rock strain distribution and strain rates

Francesco Mazzarini[*,1], Alexander R. Cruden[2], Ilaria Isola[1]

(1) Istituto Nazionale di Geofisica e Vulcanologia, Sezione di Pisa, Pisa, Italy
(2) School of Earth Atmosphere and Environment, Monash University, Melbourne, Australia

Article history: received December 16, 2024; accepted August 12, 2025

Abstract

Sheet intrusions (dikes and sills) represent the most viable mode of magma transport and emplacement within the brittle upper crust. The thickness-to-length aspect ratio of such intrusions provides information about magma emplacement mechanisms and provides information on intruded magma volumes. Within the brittle upper crust, the mobility of magma is governed by magma cooling and solidification rates. The cooling rate of sheet intrusions depends on the temperature difference between magma and its host rocks, the thickness of the intrusion and the thermal diffusivity of the surrounding crust. The cooling rate of magma in the upper crust can be expected to be faster than the tectonic strain rate. In eastern Elba Island Italy, well exposed, late Miocene leucogranite sheets that intrude schistose host rocks within the contact aureole of the Porto Azzurro pluton provide a natural laboratory for analysing sheet intrusion geometries (length, thickness, spacing between intrusions). The thickness-to-length ratios of the intrusions define a power law dimensional scaling relationship with exponent ~1. Using this length versus thickness scaling we estimate that the total volume of leucogranite that intruded the Porto Azzurro pluton contact aureole was 4-15 × 10^6 m^3. Moreover, by analysing the spacing between sheet intrusions along with the size distribution of their thicknesses, we estimate that their emplacement was accommodated by an average bulk strain (volumetric strain) of 13-15% of the Porto Azzurro pluton contact aureole host rocks. Our observations also highlight how host rock brittle structures may control the location and mode of magma emplacement. Well exposed sections of sheet intrusions and their host rocks, as observed on Elba Island, are natural laboratories where geometries of intrusions can be analysed to provide important clues on the mechanisms of magma emplacement within the brittle crust, and interactions between magmatic and deformation processes.

Keywords: Thickness, size distribution, and volume of intrusive sheets; Eastern Elba Island; Italy

1. Introduction

Emplacement of sub-horizontal tabular intrusions normally occurs via host rock brittle deformation and Mode I fracture formation (e.g. Petford et al., 2000 and references therein). Consequently, the thickness-to-length ratios of sheet intrusions are often assumed to have similar displacement-length scaling relationships to fractures (e.g. Clark and Cox, 1996; Scholz, 2002; Schultz et al., 2008a).

The thickness-to-length ratios of tabular intrusions have been used to estimate emplacement-related magma pressures or the expected thickness of intrusions by assuming a simple thin, circular elastic plate equation (e.g. Johnson and Pollard, 1973; Pollard and Johnson, 1973; Delaney and Pollard, 1981; Kusumoto et al., 2013; Biswas et al., 2023; 2025). Thickness-to-length relationships observed in the field and from geophysical data have subsequently used to provide additional insight into the mechanics of tabular intrusion emplacement (McCaffrey and Petford, 1997; Cruden et al., 2017).

Accurate estimation of the aspect ratios of tabular intrusions is therefore important for defining both the local fluid pressure (i.e. magmatic overpressure) during intrusion and the volume of emplaced magma. The dimensions of large, crustal scale tabular intrusions must typically be determined by geophysical investigations (e.g. Thomson and Hutton, 2004; Cruden and McCaffrey, 2001; Cruden, 2006; Cruden et al., 2017; Cruden and Weinberg, 2018) whereas the dimensions of medium to small scale tabular intrusions (i.e. dikes and sills) are defined by field observations and geological mapping (e.g. Rocchi et al., 2002; Mazzarini and Musumeci, 2008).

Cooling of tabular intrusions in the upper crust is a relatively rapid process, which mainly depends on the temperature difference between magma and host rock and the intrusion thickness (e.g. Annen, 2011). Since the rates magma sheet emplacement are expected to be much higher than tectonic strain rates, the emplacement of sheet intrusions is assumed to be governed by brittle deformation processes even in the ductile crust (e.g. Rivalta et al., 2015; Sassier et al., 2009). The occurrence of brittle structures, such as faults and fractures, significantly influences dike propagation (Gaffney et al., 2007; Le Corvec et al., 2013; Pagli et al., 2015). On the other hand, it has been shown that late-stage sheet intrusions in deforming crust may record different deformation fabrics depending on how strain is partitioned and the rheological heterogeneity in the host rock at the time and site of their emplacement (e.g. Papeschi et al., 2022).

In eastern Elba Island, Italy, late Miocene tabular intrusions of leucogranite are well exposed allowing detailed field observations of their geometries (Mazzarini and Musumeci, 2008; Papeschi et al., 2022).

The aspect ratios of these tabular intrusions are used here to estimate the intruded magma volume and the country rock strain induced by the magma emplacement process.

2. Geological background

Elba Island in the northern Tyrrhenian Sea is part of the Neogene northern Apennine chain (Fig. 1). The geological structure of the island is characterized by a stack of five tectonic units derived from both oceanic (Ligurian) and continental (Tuscan) domains, organized in two thrust systems (e.g. Musumeci and Vaselli, 2012; Massa et al., 2017 and references therein). The upper thrust system comprises non-metamorphosed Ligurian and Tuscan cover units (Pertusati et al., 1993; Papeschi et al., 2022 and references therein). The lower thrust system, which crops out in southeast Elba Island (Fig. 1) is made up of the metamorphic Ortano and Calamita Units, which are both derived from Mesozoic and Paleozoic rocks of the Tuscan domain (e.g. Musumeci et al., 2011; 2015; Papeschi et al., 2022 and references therein).

The architecture of the tectonic stack (Fig. 1) is characterized by several west-dipping thrust faults with top-to-the-east displacement, with the main thrust between cover and metamorphic units being located in central-eastern Elba Island (Massa et al., 2017). Stacking and deformation of the two thrust systems is related to the late Oligocene-early Miocene main deformation phases of the northern Apennine orogeny (Pertusati et al., 1993). The Monte Capanne and Porto Azzurro granitic plutons were emplaced in the Late Miocene into the nappe stack, together with systems of leucogranite sills and laccoliths (Dini et al., 2002; Mazzarini and Musumeci, 2008). The large Monte Capanne pluton in the west was emplaced ca. 7-8 Ma into the Ligurian unit of the upper thrust system (Farina et al., 2010).

The Porto Azzurro pluton, emplaced into the Calamita Unit, is only locally exposed north of the Calamita peninsula (Fig. 1). This pluton is interpreted to be much larger than its current outcrop due to the width

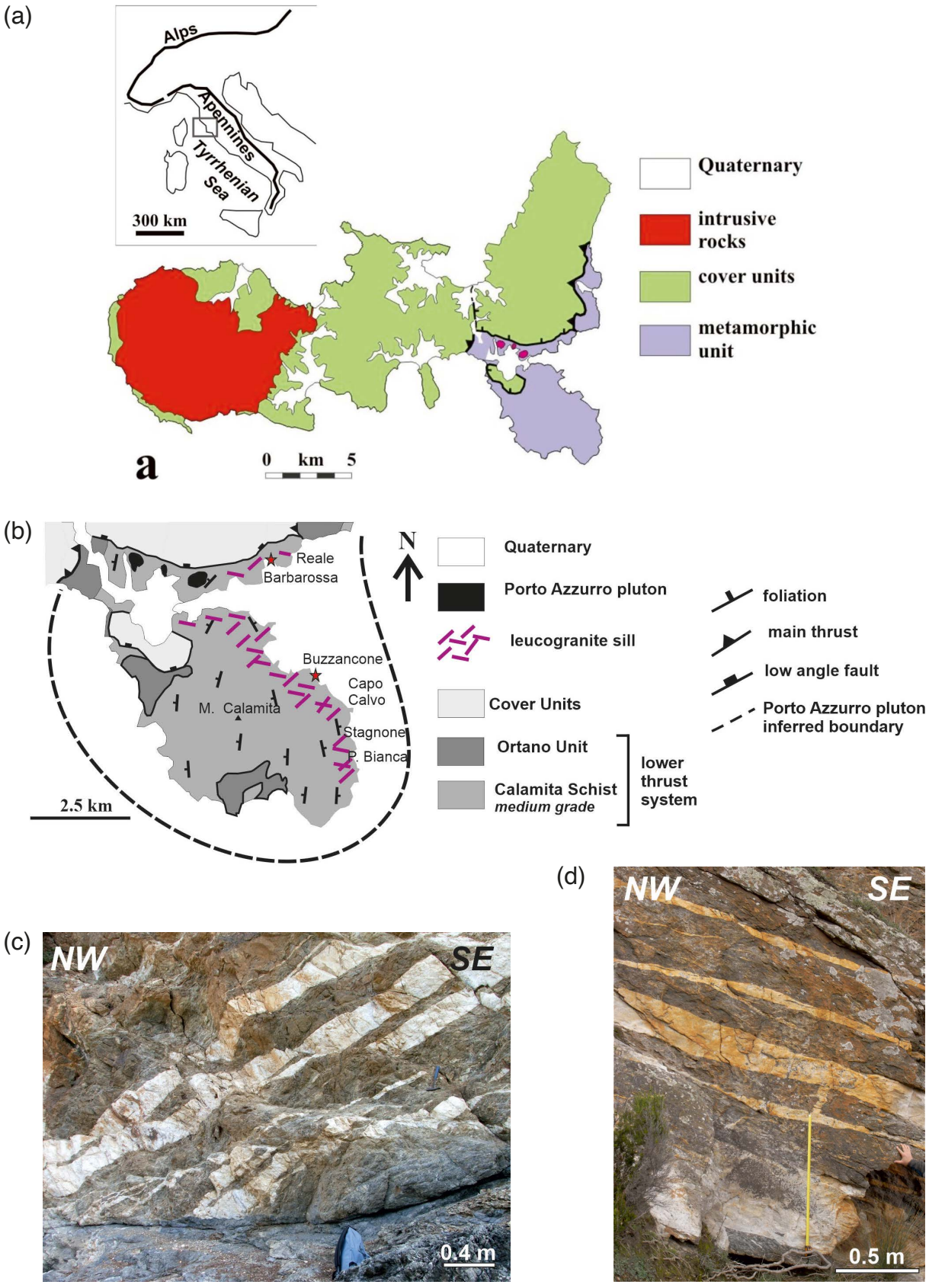

Figure 1. (a) Simplified geological map of Elba Island, and geodynamic framework (inset), CP: Calamita Peninsula. Thick black lines with triangles: main thrusts; thin black lines with segments: low angle faults. (b) Simplified geological map of the study area (after Mazzarini and Musumeci, 2008 and Cruden et al., 2009). (c) Photographs of sills intruding the host rock at the Barbarossa site (red star in Fig. 1a). (d) Photographs of sills intruding the host rock at the Buzzancone site (red star in Fig. 1a).

of its contact aureole and the distribution of associated leucogranitic sheets hosted in pelitic–psammitic hornfels host rocks (Calamita Schist) in the Calamita Peninsula (e.g. Mazzarini and Musumeci, 2008).

The Calamita Schist, which hosts the Porto Azzurro pluton, consists of medium-to-high grade hornfels with biotite+muscovite+andalusite+cordierite+K-feldspar mineral assemblages (Papeschi et al., 2017). The contact metamorphic parageneses in the Calamita Schist contain cordierite and/or andalusite assemblages indicating a maximum paleo-depth of emplacement <10 km (P < 0.2-0.3 GPa) and metamorphic temperatures ranging from 450-500 °C to more than 650-700 °C (Duranti et al., 1992; Musumeci and Vaselli, 2012; Papeschi et al., 2019). Throughout the Calamita peninsula, the metamorphic grade increases eastward and the innermost portion of the contact aureole of the Porto Azzurro pluton (pyroxene hornfels facies) crops out along the east coast coincident with the occurrence of leucogranitic sheet intrusions derived from the pluton.

The exposed igneous rocks of the Porto Azzurro pluton have yielded ages of 6.53 ± 0.39 Ma (U–Pb zircon; Gagnevin et al., 2011), 6.4 ± 0.4 Ma and 6.4 ± 0.3 Ma (U–Pb zircon; Spiess et al., 2021), a continuous age spectrum between 6 and 7 Ma (U-Pb zircon; Mazzarini et al., 2024), 6.33 ± 0.67 Ma ($^{40}Ar/^{39}Ar$ muscovite; Musumeci et al., 2015), 5.9 ± 0.2 Ma ($^{40}Ar/^{39}Ar$ biotite; Maineri et al., 2003), and a 5.6-6.0 Ma age spectrum ($^{40}Ar/^{39}Ar$ muscovite; Mazzarini et al., 2024). Low pressure-high temperature (LP-HT) metamorphic minerals in the Calamita Unit range between 6.76 ± 0.08 Ma ($^{40}Ar/^{39}Ar$ phlogopite), 6.40 ± 0.15 Ma (U–Pb zircon; Musumeci et al., 2011), 6.23 ± 0.06 Ma ($^{40}Ar/^{39}Ar$ muscovite; Musumeci et al., 2015).

The wide contact aureole of the Porto Azzurro pluton contains a regional asymmetric anticline, with steeply dipping axial plane and a gently north plunging fold axis (Cruden et al., 2009; Mazzarini et al., 2011; Papeschi et al., 2017). Geophysical investigations in the northern Calamita peninsula have defined the occurrence of the Porto Azzurro pluton at very shallow depths (100-200 m) below the surface (Siniscalchi et al., 2008). The maximum elevation (~420 m) along an E-W transect across the Calamita peninsula is assumed to provide a rough estimate of the contact aureole thickness without the contribution of late magmatic, leucogranitic sheet intrusions.

The late stage leucogranitic sheet intrusions on eastern Elba Island display variable angular relationships with the host rock foliation from discordant, with angles >40°, to para-concordant (angles ≤10°); in general, they are never fully concordant with the host rock foliation (Mazzarini and Musumeci, 2008). Mazzarini and Musumeci (2008) and Cruden et al. (2009) suggested that these late stage intrusions exploited already formed fracture systems. Recent detailed analysis of the geometric relationships between rock foliation and the orientations of sheet intrusions and their internal fabrics indicate that late-stage leucogranitic intrusions were emplaced into the contact aureole of the Porto Azzurro pluton during crustal shortening (Papeschi et al., 2017; 2021; 2022). Although generally discordant with the main host rock structure, because the leucogranitic sheet intrusions in eastern Elba Island mostly dip gently (Cruden et al., 2009; Papeschi et al., 2022), we will refer to them here as sills.

3. Geometric scaling of sheet intrusions

Empirical dimensional scaling data from tabular igneous intrusions has been employed to understand emplacement mechanisms, to determine the initiation conditions and driving pressures of intrusive sheets and to discriminate between propagation regimes predicted by Linear Elastic Fracture Mechanics (Cruden et al., 2017 and references therein). Dimensional scaling has also been used for defining deformation mechanisms during the formation of brittle structures at micro- to crustal scales (Schultz et al., 2008b).

Displacement-length scaling of faults, joints, veins, dikes, shear bands and compaction bands is generally defined by a power-law:

$$d = bl^a \tag{1}$$

where d is the maximum displacement (i.e. slip for a faults and thickness for dikes, etc.), l is the length, a is a power-law exponent and b is a normalization constant.

Generally, two scaling categories have been defined (Schultz et al., 2008a): faults and shear bands are characterized by $a \sim 1$, and opening and closing structures (i.e. veins, dikes, compaction bands) have power-law slopes with $a \sim 0.5$. According to Linear Elastic Fracture Mechanics (LEFM), $a \sim 1$ implies fracture propagation with constant opening driving stress $\Delta\sigma_o = P_f - \sigma_n$, (where σ_n is the stress normal to the crack wall and P_f is the fluid pressure), and $a \sim 0.5$ implies that fracture toughness (K_{Ic}) governs fracture propagation (Olson, 2003).

Constant aspect ratios are expected for a~1, while aspect ratio scaling with length is expected for a~0.5. The propagation and emplacement of sills and dikes is normally assumed to occur via opening mode fractures (Mode I), and the fracture aperture (or thickness) t replaces the displacement d in Eq. (1).

Cruden et al. (2017) analysed a large database of tabular igneous intrusions, emplaced in different geo-tectonic environments, having different compositions and with lengths and thicknesses spanning multiple orders of magnitude. It emerges from this large database that the thickness-to-length ratio (representing the intrusion's growth behavior) increases for a < 1 (i.e., lengthening outpaces thickening) while for $a > 1$ the aspect ratio decreases while thickening becomes prevalent (Cruden et al., 2017).

The aspect ratios of tabular igneous intrusions vary greatly depending on emplacement processes, crustal depth and magma composition (e.g. Cruden et al., 2017), and for dikes and sills is best represented by a~0.5.

Field measurement of the length of sheet intrusions (i.e. tip-to-tip dimension) is often affected by bias introduced by measuring intrusion dimensions on generally two-dimensional exposures, which can result in underestimation of the true length (e.g. Biswas et al., 2025).

Considering that two-dimensional length measurements are random samples (cords) through disk-shaped intrusions (Fig. 2), it is theoretically possible to correct for measurement bias in the data (e.g. Cruden et al., 2009). However, to avoid this sampling problem we explore whether information on the mechanics of sub-horizontal tabular intrusion emplacement can be derived from measurements of thickness alone.

The length of sills and dikes is difficult to measure because true diameters (or major axes for ellipses) are often not observed in the field (e.g. Cruden et al., 2009). Conversely, the thickness of tabular intrusions is often well defined by direct observations. We model tabular intrusions (sills) as two parallel disks that meet at a rapidly tapering tip (Fig. 2). The tip region (b) is much shorter than the diameter (r) or any chord (c) across the sill (Fig. 2). In this model r or $c \gg b$ so any thickness sampled along a chord at a distance from the tip $> b$ will be very close to the true maximum thickness (t).

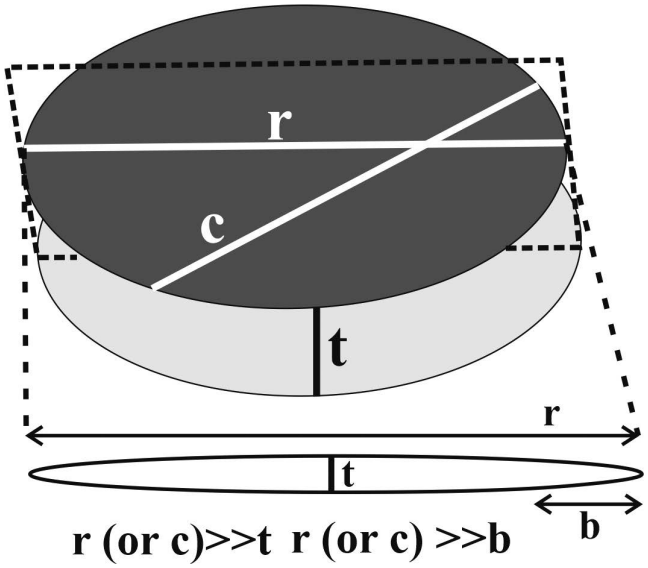

Figure 2. Conceptual model for a dike or sill bounded by two parallel disks with radius (r). The dike or sill thickness, $t \ll r$ is nearly constant across a section along the diameter (dashed plane) or across any chord (c). The tip region (b) is very short compared to any diameter or chord across the intrusion.

According to Cruden et al. (2017), the volume (V) of a sill is

$$V = \pi t \left(\frac{l}{2}\right)^2 \tag{2}$$

where t and l are the thickness and length of the tabular intrusions.

According to Eq. (1):

$$l = \left(\frac{t}{b}\right)^{\frac{1}{a}}$$

And substituting l into Eq. (2):

$$V = \pi t \left(\frac{t}{2b}\right)^{\frac{2}{a}} \quad (3)$$

gives a volume estimate that depends on the thickness.

4. Geometric scaling relationships of leucogranite sills in eastern Elba Island

Initial measurements of the tip-to-tip lengths and the maximum thicknesses of sixty-nine leucogranite sills were collected in the field in eastern Elba Island (Table 1). Tip-to-tip lengths were acquired by using tape measure and, in case of very large sills, by analysing composite panoramas from photographs. Lengths <60 m taken from a tape measure have an uncertainty of ±5 cm. Lengths >60 m measured by image analysis have an uncertainty of ±3 m. True thickness measurements were all collected using a tape measure and have an uncertainty of ±0.1 cm. Spacing between sills was also determined using a tape measure with an uncertainty of ±0.5 cm.

Estimating the true spacing between and thickness of inclined sills (light grey stripes in Fig. 3) along outcrop sections requires the line normal to the sills to be defined (dashed line in Fig. 3). The following parameters are used: the length of the field measurement section (L_{fms}), the thickness of (t_{ms}) and the spacing (s_{ms}) between sills measured along the field section; α is the angle between the normal to sills and the field section; t_i and s_i are the projected true thickness and spacing, respectively (Fig. 3).

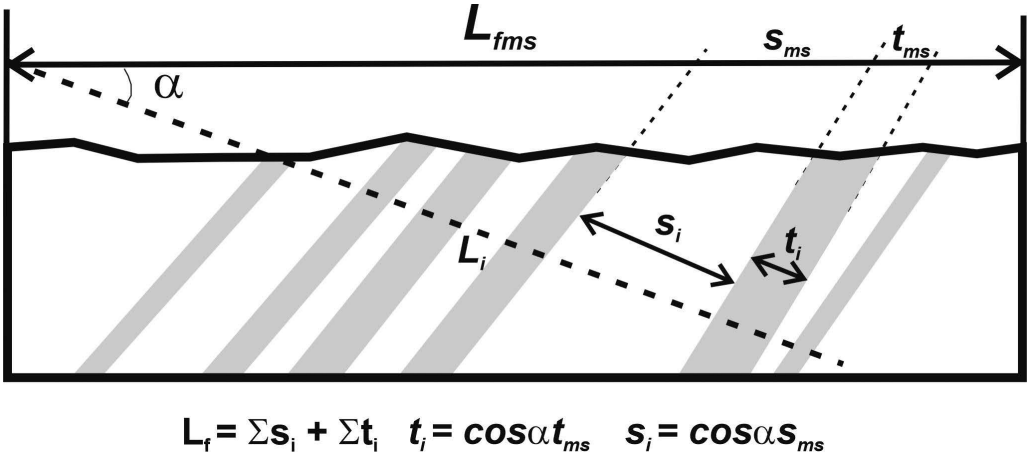

Figure 3. Diagram showing the method used to estimate the true spacing between and thickness of leucogranitic sills (light grey stripes) exposed along outcrop sections on eastern Elba Island. The dashed line is the line normal to the sills; L_{fms}, t_{ms} and s_{ms} are the field measurements of the outcrop section length, and sill thickness and spacing, respectively, *Li* is the projected length of the section length; α is the angle between the normal to sills and the field outcrop section, t_i and s_i are the projected true thickness of and spacing between sills, respectively.

Subsequent field campaigns along the east coast of the Calamita Peninsula provided additional data comprising 193 measurements of sill thickness and 139 measurements of sill spacing (Table 2). These new data were mainly acquired along transects at several sites, a few hundreds of meters apart, containing the greatest exposure and concentration of sills, taking care to avoid repeat measurements of sills at each site.

Table 1. Statistics of the initial 69 measurements of length (l), thickness (t) of sills.

	l (m)	t (m)	l/t
Max (m)	175	6.820	290.0
Min (m)	0.92	0.025	4.725
Mean (m)	19.40	0.600	55.2
St. dev (m)	34.90	1.100	52.6

The leucogranite sills in eastern Elba Island have a maximum exposed length of 175 m (Table 1) and most of sills have gentle-to-low dips (e.g. Cruden et al., 2009).

Table 2. Statistics of additional 193 sill thicknesses (t) and 139 spacing (sp) measurements of sills.

	t (m)	sp (m)
Max (m)	6.82	18.3
Min (m)	0.003	0.02
Mean (m)	0.364	1.53
St. dev (m)	0.764	2.47

4.1 Thickness and spacing size distributions

The eastern Elba Island leucogranite sills are discordant or para-concordant to the main foliation in the host rock (Fig. 1c, 1d; Mazzarini and Musumeci, 2008; Cruden et al., 2009; Papeschi et al., 2022) and have parallel, straight walls and, where observed, the tip regions are very short and rapidly tapered. Hence these sills fit the proposed model for tabular intrusion geometry (Fig. 2), which implies that their observed thicknesses will be very close or equal to the true sill thickness.

The arithmetic mean of the additional sill thickness data is 0.36 m (Table 2) and they range from 0.003 to 6.8 m.

The size distributions of the sill thickness and spacing measurements can be defined by a power law (Fig. 4):

$$g(t) = \gamma t^{D} \tag{4}$$

where D is the power-law exponent and γ is a normalization constant.

According to Eq. (4), the observed thickness distribution for the Calamita sills (193) is defined by a power-law $n(>t) = 11.667t^{-1.1942}$, with a regression coefficient, $R^2 = 0.9817$ for sills with thicknesses between 0.2 and 2.5 m (Fig. 4a). The theoretical maximum thickness of the distribution, TMAX = 7.8 m, is very close to the maximum observed thickness, TM of 6.8 m, suggesting that truncation and censoring do not strongly affect the data.

The measured spacing between sills (139) ranges range between 0.02 and 18.3 m, with an average value of 1.53 m (Table 2). According to Eq. (4), the spacing distribution is defined by a power-law $n(>\text{sp}) = 59.51\text{s}^{-1.1352}$, with $R^2 = 0.9610$, for sill spacing values between 1 and 9 m (Fig. 4b). The computed maximum value of the sill spacing,

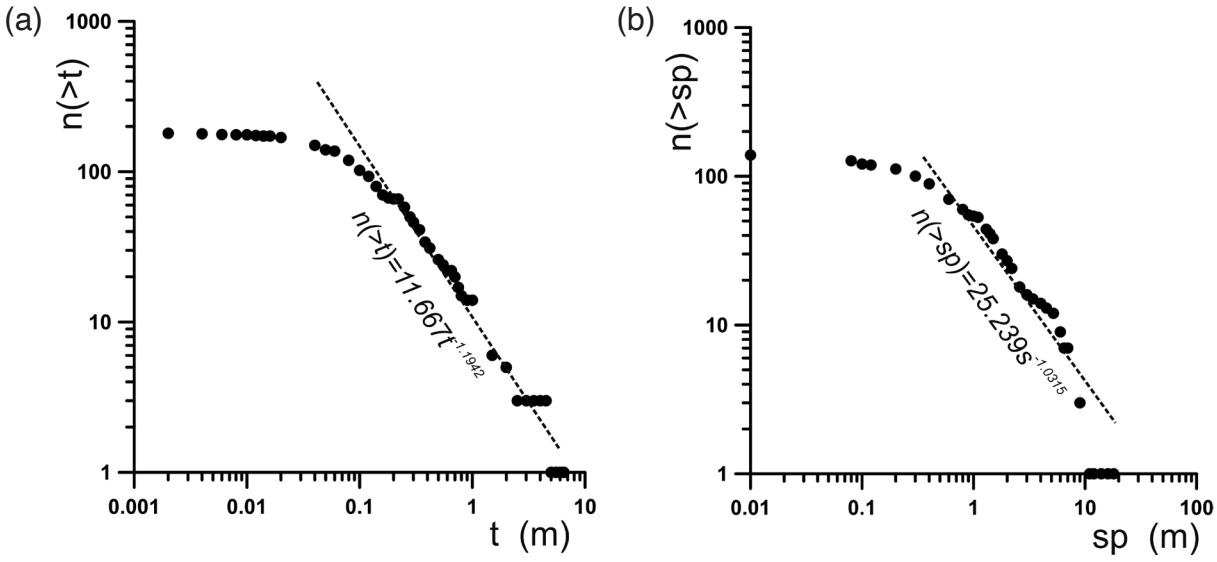

Figure 4. (a) Plot of $n(>t)$ vs. thickness (t), and (b) plot of $n(>s)$ vs. spacing (s) measurements of leucogranitic sills exposed on eastern Elba Island.

SMAX for $n(>s) = 1$ is 36.6 m. This value is twice that of the observed maximum value (18.3 m), suggesting that the data set is affected by censoring and that widely spaced sills are underestimated.

The cumulative distribution for the thickness, t, (and for spacing, s) of leucogranitic sills can be generally defined as:

$$n(t) = \int_{t}^{TM} g(t)\delta t \tag{5}$$

where $n(t)$ is the number of sills with thickness greater than t, TM is the maximum thickness in the population, and $g(t)\delta t$ is the number of sills in the interval $t + \delta t$.

The average sill thickness value is:

$$\bar{t} = \frac{-\int_{tm}^{TM} -\gamma D x^{-(1+D)} x dx}{\gamma t m^{-D} - \gamma T M^{-D}} = \frac{D\left[x^{(1-D)}\right]_{tm}^{TM}}{(1-D)(tm^{-D} - TM^{-D})} \tag{6}$$

where D and γ are the parameters from the power-law size distribution Eq. 4 (see Mazzarini et al., 2010; 2014).

For the leucogranitic sills exposed on the Calamita peninsula of eastern Elba Island the mean thickness of the population derived from Eq. (6) is 0.04 m less than the arithmetic mean (Table 2). This is consistent with the observed power-law size distribution value $D > 1$, which implies that the thickness distribution is controlled by thin sills. The mean sill spacing from Eq. (6) is 0.9 m less than the arithmetic mean (Table 2).

Using the thickness distribution for the leucogranitic sills, and assuming a minimum thickness (tm) of 0.001 m, gives a maximum cumulative thickness of ~170 m. This estimate of the cumulative thickness assumes that all sills are stacked one above the other within a vertical section. However, this scenario is not realistic given the uneven distribution of sills in eastern Elba Island (e.g. Cruden et al., 2009) and the dependence of the spatial distribution of the sills on their spacing.

4.2 Thickness-Length scaling

The l and t values (69) of leucogranite sills are positively correlated on a log-log plot (Fig. 5a) defining a best-fit power-law with a = 0.8409 and b = 0.03456 (Eq. 1). The l/t ratio has a dispersed distribution in a log(l)-log(l/t) plot, where it is difficult to define a clear trend (Fig. 5b).

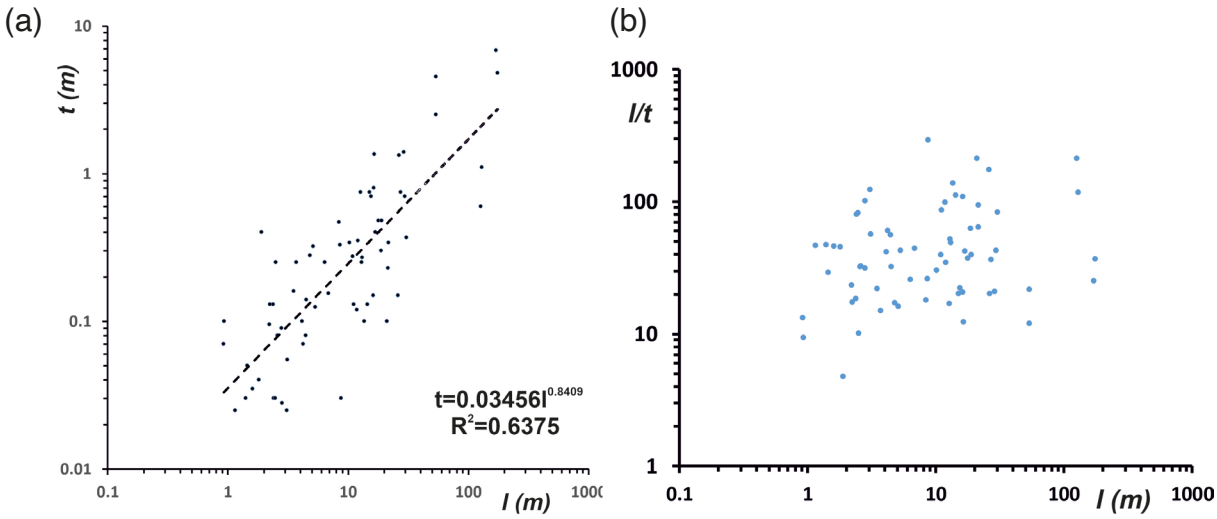

Figure 5. Length and thickness measurements (69) of the sills at eastern Elba Island. (a) Plot of length (l) vs. thickness (t); (b) plot of sill length (l) vs. aspect ratio (l/t).

There is no a priori reason for an asymmetrically distribution of errors in l and t, thus the Reduced Major Axis Regression (RMA) (Davis, 2002; Smith 2009) is also used along with the ordinary least squares method to define the parameter scaling law parameters in Eq. (1). The RMA analysis provides a = 0.991 and b = 0.02593.

The standard error of regression (S) of the computed a value and the goodness of fit have been evaluated for the regression of the data by imposing fixed value for the exponent for power law and RMA fits (Table 3). The distribution of residuals of fit is computed for a = 0.8409 (Fig. 6a) and a = 0.9 (Fig. 6b). The best fit is obtained by using the exponent 0.9 and also by the RMA fit (Table 3).

Table 3. Regression parameters for the measured l-t data; a and b are the parameters in Eq. (1). Pl: power-law fit; RMA: Reduced Major Axis; S: standard error of regression.

Method	a	b	S
pl	0.5	0.2181780	0.819162
pl	0.8409	0.0559654	0.696105
pl	0.9	0.0426446	0.692420
RMA	0.991	0.0259320	0.693229

The power-law exponent $a = 0.9$ is greater than the value expected for sills (0.5) and is close to the values expected for some plutons and layered mafic intrusions (Cruden et al., 2017).

The deviation of the scaling exponent for eastern Elba leucogranite sills (~1) from the theoretical value of 0.5 (Cruden et al., 2017) suggests that the thickness-to-length ratio of these sheet intrusions could result from a growth mechanism that was not controlled by the host rock fracture toughness.

Recent models for the growth of sheet intrusions (Gill et al., 2022) frame the final thickness-to-length ratio in terms of a competition between kinetic dominated (non-stationary) and toughness dominated (stationary) processes. In the model of Gill et al. (2022), dikes extend their length in two stages: an initial inflation stage in which both length and thickness increase and a final, constant volume relaxation stage where length can only grow at the expense of the maximum thickness. Cooling and solidification processes (e.g., Annen, 2011) may also exert a strong control on dyke lengthening (Gill et al., 2022). In eastern Elba Island, the leucogranite sheets are estimated to have solidified very quickly (Papeschi et al., 2022) suggesting that the relaxation stage of the Gill et al. (2022) model

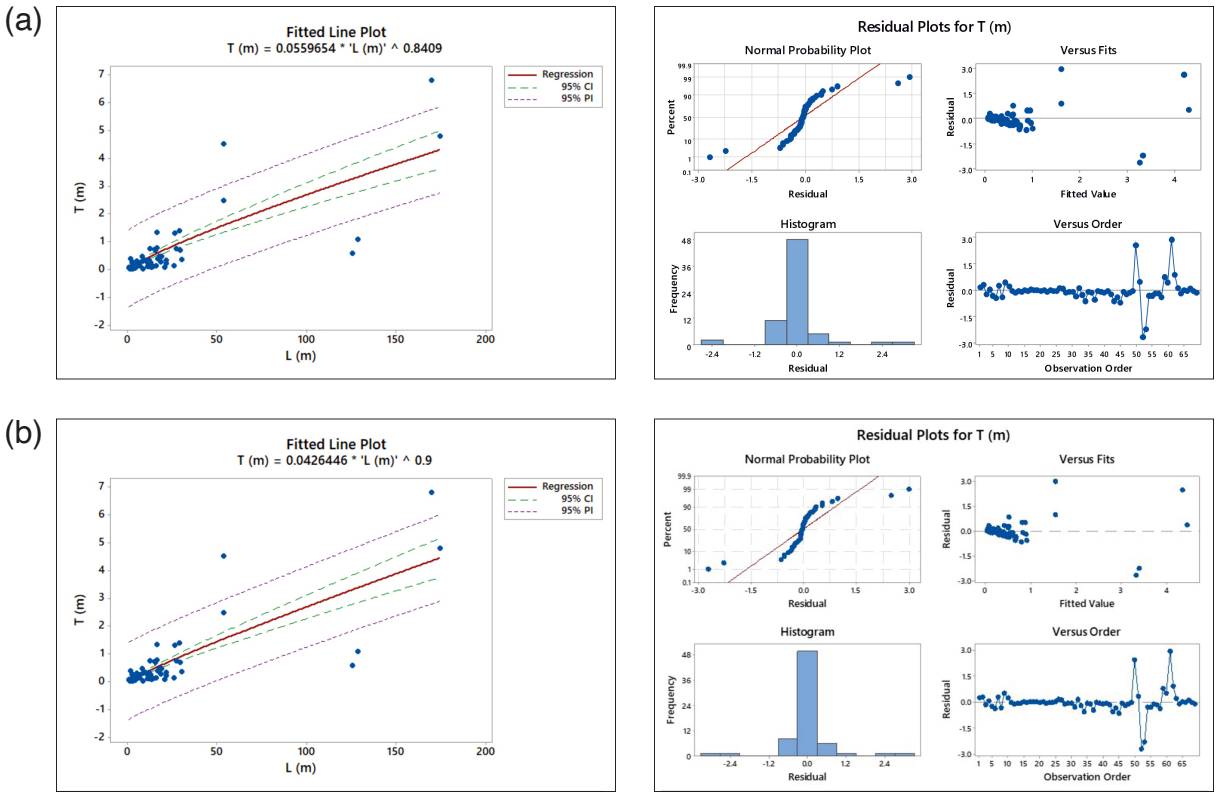

Figure 6. (a) left panel: Plot of sill length (l) vs. thickness (t) with 95% confidence (CI) and probability (PI) intervals for a power law with a = 0.8409; right panel: plot of distributions of residuals of the power-law fit. (b) left panel: Plot of sill length (l) vs. thickness (t) with 95% confidence (CI) and probability (PI) intervals for a power law with a = 0. 9; right panel: plot of distributions of residuals of the power-law fit.

likely operated over a short time, leading to a higher-than-expected power law scaling exponent a~1. Notably, in the Calamita Peninsula, the sheet intrusions were emplaced within a deforming host rock by exploiting extensional shear fractures (Cruden et al., 2009; Papeschi et al., 2017; 2022), consistent with the model of Gill et al. (2022).

4.3 Volume of magma intruded into the Porto Azzurro pluton contact aureole

The cumulative volume of magma intruded into the contact aureole of the Porto Azzurro pluton can be estimated using the length vs thickness scaling relationships (Table 3) and Eq. (3) and (4).

The volume of a single sheet with thickness t is computed according to Eq. (3) and then it is multiplied by the number $g(t)$ from Eq. (4). The starting t value has been fixed to 0.003 m, that is a thickness for which the igneous nature of a leucogranite sill is clearly visible in the field (occurrence of small grains of biotite and/or tourmaline), and the maximum thickness is set to the maximum theoretical value of 7.8 m.

The resulting estimated magma volume is 3.99×10^6 m^3. This value may rise to 15×10^6 m^3 if several sills with thickness larger than 5 m are added to the calculation. The latter case may be representative of several large sills that are missing due to censoring effects in the spacing estimation. Notably, if power law scaling exponent a = 0.5, typical for small sills (e.g. Cruden et al., 2017), is used the same calculation yields an unrealistic magma volume of 2.8×10^{-11} m^3 and a cumulative thickness of ~1.87 km instead of the estimated 170 m (see section 4.1).

5. Host rock strain due to magma emplacement

The addition of leucogranitic sills into the contact aureole of the Porto Azzurro pluton increased the host rock thickness to its current value (T_f).

Using the cumulative distributions of leucogranite sheet thickness and spacing, we estimate the T_f value using Eq. (4) and by calculating the number of sills in the observed 0.003-6.8 m thickness range. Next we multiply the cumulative number of sills by the average sill thickness (0.04 m) and divide by the average sill spacing (0.9 m) from Eq. (6). This gives an estimated value of T_f of ~530 m.

In eastern Elba Island, the occurrence of high temperature metamorphic assemblages in the host rocks of the leucogranite sills suggests that they were emplaced close to the roof of the Porto Azzurro pluton (e.g. Siniscalchi et al., 2008; Musumeci and Vaselli, 2012; Papeschi et al., 2019). Considering the current maximum elevation of the Calamita Schists (~400 m above sea level) and the depth of the contact with the granite derived from geophysical data (Siniscalchi et al., 2008), the contact aureole must have been 500-600 m thick, which is in close agreement with our T_f estimate.

The above analysis indicates that the contact aureole of the Porto Azzurro pluton was intruded by a maximum cumulative thickness of ~170 m of leucogranitic magma.

At any location within the aureole, the addition of magma via sheet intrusions increased the local host rock thickness according to $T_f = T_i + T_s$ and thus the local percentage host rock strain is:

$$\varepsilon = 100x\frac{T_f - T_s}{T_i} = 100x\frac{T_s}{T_i} \tag{7}$$

where T_f is the final contact aureole thickness (500-600 m, see above), T_i the initial contact aureole thickness and T_s the cumulative sill thickness, in which the initial thickness of the contact aureole can be assumed to be ~400 m thick.

The strain in the contact aureole has been evaluated at 6 localities on the Calamita Peninsula (Fig. 7) by calculating the cumulative thickness of sills along transects, taking into account of their orientation and projecting their thickness and spacing along a line normal to the average sill dip (Fig. 3).

The average number of stacked leucogranitic sills in the contact aureole of the Porto Azzurro pluton is found by dividing the contact aureole thickness (T_i) by the average sill spacing (S_m). The cumulative sill thickness (T_s) is can then be obtained from:

$$T_s = T_{sm}\frac{T_i}{S_m} \tag{8}$$

where T_{sm} is the mean thickness of sills. The local percentage strain in the contact aureole is computed using Eq. (7).

The field measurement transects at the localities indicated in Fig. 7 vary in length from 0.8 to 49 m and give a large range in percentage strain from 1 to 51%, in which the lowest strains are observed in the longer transects (Fig. 8a). Percentage strain between 10 and 51% is computed along transects with lengths that are less than twice the average sill spacing (i.e. ~0.9 m).

Percentage strain in transects longer than twice the average sills spacing (~2.0 m) ranges from 4 to 33% (Fig. 8b). The longer transects are considered less affected by local effects (e.g. thin frequent sills) and in this subgroup we estimate an average percentage strain of 12% with a range of 4 to 26%. The most frequent value (mode) of strain is 13%. In each transect, the ratio between the transect length and the cumulative sill thickness varies between 0.51 and 1, with an average of 0.24, and the ratio for the longest transect is 0.098. The data in Fig. 7 indicate a heterogeneous distribution of the strain within the contact aureole.

From Eq. (6), the eastern Elba Island leucogranitic sills have average thickness and spacing of 0.04 m and 0.9 m, respectively. Therefore, the host rock strain derived by combining Eq. (6) and (7) ranges between 4 and 20%, which is very similar to that observed in the field.

The timing of leucogranitic sill intrusion within the contact aureole of the Porto Azzurro pluton can be constrained from existing geochronological data (see Geological background section). $^{40}Ar/^{39}Ar$ data on leucogranitic sills suggest that they were emplaced over a time span of ca. 0.73 Myr (6.33-5.6 Ma; Musumeci et al., 2015; Mazzarini et al., 2024). Using the estimated percentage strain range (1%-51%) gives a strain rate of 2.2×10^{-14} to 4.3×10^{-16} s^{-1}, which is comparable to established tectonic strain rates of 10^{-13} and 10^{-15} s^{-1} (e.g. Pfiffner and Ramsey, 1982; Paterson and Tobisch, 1992).

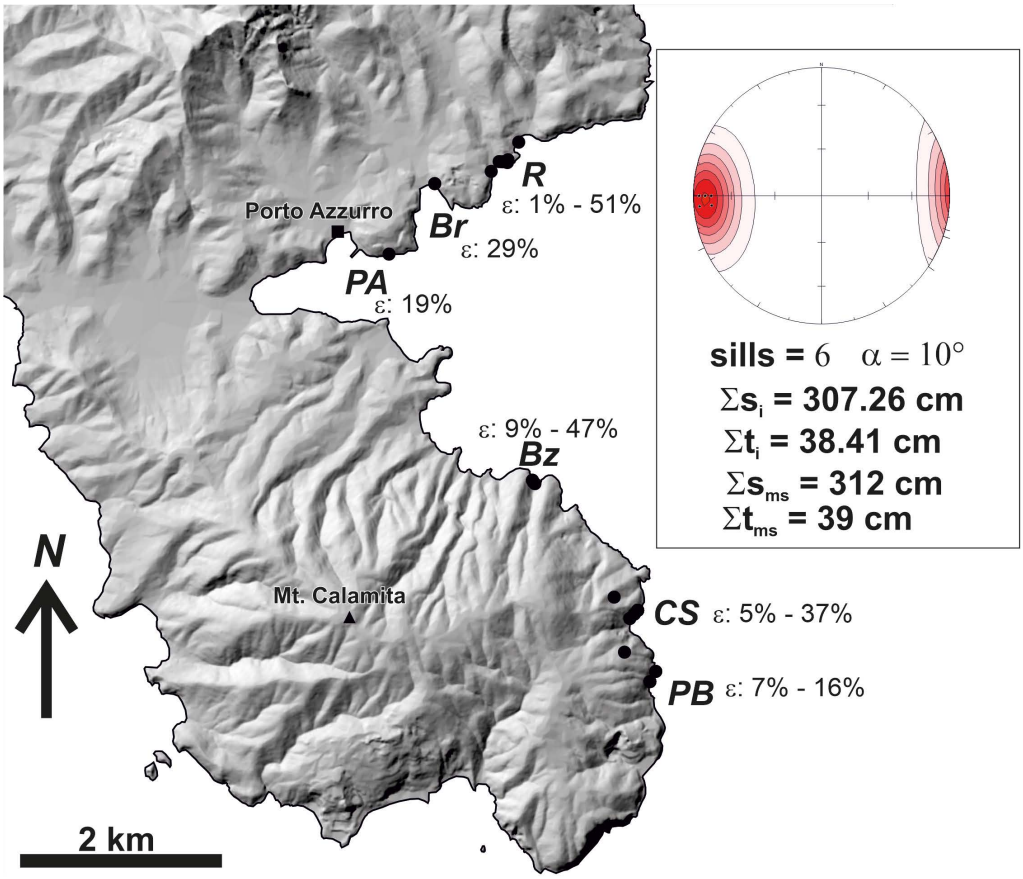

Figure 7. Map with locations of sections for the estimation of host rock strain. R: Reale; B: Barbarossa; PA: Porto Azzurro; Bz: Buzzancone; CS: Cala Stagnone; PB: Punta Bianca. The range of the measured percentage strain (ε) is reported for each site. Inset is a lower hemisphere stenographic projection plotting poles to sills measured at the Cala Stagnone transect – the maximum concentration of poles defines the mean orientation of a line normal to sills onto which field measurements are projected (see Fig. 3 for explanation).

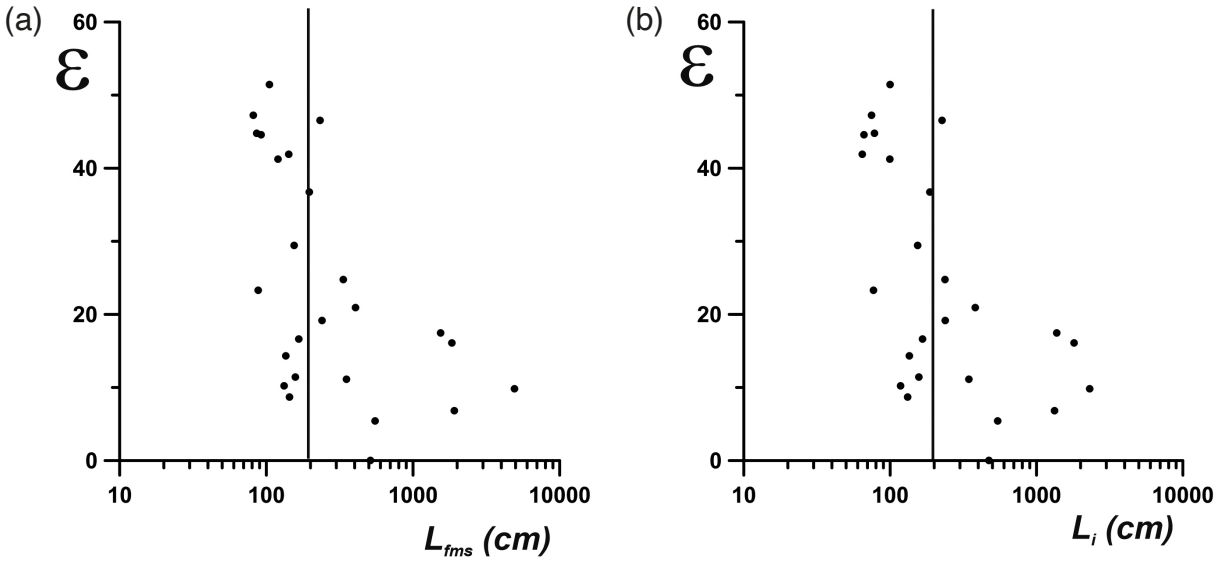

Figure 8. (a) Semi log plot of the % strain (ε) vs. the length of the field measurement transect (L_{fms}). The solid black line separates transects with lengths less than and greater than 2 m (i.e. twice the average sill spacing). (b) Semi log plot of the percentage strain (ε) vs. the length of the projected transect (L_i). The solid black line separates transects with lengths less than and greater than 2 m (i.e. twice the average sill spacing).

6. Discussion and Conclusions

The geometric scaling of tabular intrusions provides insights on the emplacement mechanism of leucogranite sills in eastern Elba Island. The thickness-to-length ratio of the sills indicates that their thickness scales with length with a power law exponent $a = 0.9$ (a~1; Table 3), and not 0.5 as observed for other small-scale tabular intrusions (Cruden et al., 2017). This is consistent with magma exploiting extensional shear fractures during deformation of the host rock during sill emplacement (Cruden et al., 2009; Papeschi et al., 2017; 2022). Notably, the a value is also less than 1.5, which is the value reported for granitic laccoliths exposed in western Elba Island (Rocchi et al., 2002). The power law scaling exponent $a \sim 1$ is consistent with a two-stage kinetic model of magma sheet emplacement (Gill et al., 2022); after an initial inflation stage characterised by lengthening and widening of the intrusion, a final relaxation stage takes place and the magma propagates within the fracture increasing its length before cooling and solidification arrests further growth.

The estimated volume of magma intruded via sills within the contact aureole of the Porto Azzurro pluton is between 0.001 and 0.1 km^3. Overall, field observations indicate that emplacement of leucogranitic sheet intrusions within the contact aureole of the Porto Azzurro pluton resulted in a heterogeneous strain distribution, while at the scale of the whole pluton the average percentage strain was 13-15%.

Our observations suggest that faulted/fractured media behave differently during magma emplacement compared to relatively intact host rocks because pre-existing brittle structures control the location and dynamics of igneous sheet intrusion.

Giving the short time required for cooling and solidification of tabular intrusions (Annen, 2011; Papeschi et al., 2022) the estimated strain rate associated with leucogranitic sill emplacement in eastern Elba Island is 10^{-14}-10^{-16} s^{-1}. This is a maximum value because it is unlikely that all sheet intrusions in the contact aureole were emplaced at the same time. To assess more local strain rates, the emplacement ages of all measured sheet intrusions would need to be known.

Natural exposures of sheet intrusions, as exposed in eastern Elba Island, allow the collection of extensive field data, which can provide important information on magma emplacement mechanisms, strain rates, and the geometric scaling of igneous intrusions in fractured media. Such data sets should also be valuable to place constraints on future numerical models of magma intrusion in the Earth's crust.

References

Annen, C. (2011). Implications of incremental emplacement of magma bodies for magma differentiation, thermal aureole dimensions and plutonism–volcanism relationships, Tectonophysics, 500, 3-10, doi:10.1016/j.tecto.2009.04.010.

Biswas, S. K., K. Saha, G. Das and T. K. Mondal (2023). Estimation of magma overpressure from partially exposed dykes – A new approach, J. Struct. Geol., 168, 104822a, doi:10.1016/j.jsg.2023.104822.

Biswas, S. K., T. K. Mondal, A. Saha, A. K. Mukhopadhyay et al. (2025). Estimating complete dyke dimensions from partial exposures, J. Struct. Geol., 192, 105350, doi:10.1016/j.jsg.2025.105350.

Clark, R. M. and S. J. D. Cox (1996). A modern regression approach to determining fault displacement-length relationships, J. Struct. Geol., 18, 147-152.

Cruden, A. R. (2006). Emplacement and growth of plutons: implications for rates of melting and mass transfer in continental crust, in M. Brown and Rushmer T. (Eds.) Evolution and differentiation of the continental crust, Cambridge University Press, 455-519.

Cruden, A. R. and K. J. W. McCaffrey (2001). Growth of plutons by floor subsidence: Implications for rates of emplacement, intrusion spacing and melt-extraction mechanisms, Phys. Chem. Earth, A, 26, 303-315, doi:10.1016/S1464-1895(01)00060-6.

Cruden, A. R., F. Mazzarini, A. P. Bunger and G. Musumeci (2009). Geometry, scaling relationships, and emplacement dynamics of ca. 6 Ma shallow felsic sill complex, Calamita Peninsula, Elba Island, Italy, EOS Trans., AGU, 90, Abstract, T13A, 1843.

Cruden, A. R., K. J. W. McCaffrey and A. P. Bunger (2017). Geometric scaling of tabular igneous Intrusions: Implications for emplacement and growth, in C. Breitkreuz and S. Rocchi (Eds.) Physical Geology of Shallow Magmatic Systems, Adv. Volcanol., Springer, Cham, doi:10.1007/11157_2017_1000.

Cruden, A. R. and R. F. Weinberg (2018). Mechanisms of Magma Transport and Storage in the Lower and Middle Crust – Magma Segregation, Ascent and Emplacement, in S. Burchardt (Ed.) Volcanic and Igneous Plumbing Systems: Understanding Magma Transport, Storage, and Evolution in the Earth's Crust, 13-53, doi:10.1016/B978-0-12-809749-6.00002-9.

Davis, J. C. (2002). Statistic and data analysis in geology, J. Wiley and Sons, NY, USA, 3rd ed., 638.

Delaney, P. T. and D. D. Pollard (1981). Deformation of host rocks and flow of magma during growth of minette dikes and breccia-bearing intrusions near Ship Rock, New Mexico, U. S. Geol. Surv. Prof. Pap., 1202, 61.

Dini, A., F. Innocenti, S. Rocchi, S. Tonarini et al. (2002). The magmatic evolution of the late Miocene laccolith–pluton–dyke granitic complex of Elba Island, Italy, Geol. Mag., 139, 257- 279, doi:10.1017/S0016756802006556.

Duranti, S., R. Palmeri, P. C. Pertusati and C. A. Ricci (1992). Geological evolution and metamorphic petrology of the basal sequence of eastern Elba (complex II), Acta Vulcanologica, 2, 213-229.

Farina, F., A. Dini, F. Innocenti, S. Rocchi et al. (2010). Rapid incremental assembly of the Monte Capanne pluton (Elba Island, Tuscany) by downward stacking of magma sheets, Geol. Soc. Am. Bull., 122, 1463-1479, doi:10.1130/B30112.1.

Gaffney, E. S., B. Damjanac and G. A. Valentine (2007). Localization of volcanic activity: 2. Effects of pre-existing structure, Earth Planet Sci. Lett., 263, 3-4, 323-338, doi:10.1016/j.epsl.2007.09.002.

Gagnevin, D., J. S. Daly, M. S. A. Horstwood and M. J. Whitehouse (2011). In-situ zircon U–Pb, oxygen and hafnium isotopic evidence for magma mixing and mantle metasomatism in the Tuscan Magmatic Province, Italy Earth Planet Sci. Lett., 305, 1-2, 45-56, doi:10.1016/j.epsl.2011.02.039.

Gill, S. P. A., R. J. Walker, K. J. W. McCaffrey and C. Greenfield (2022). No unique scaling law for igneous dikes, J. Geophys. Res., Solid Earth, 127, e2022JB024120, doi:10.1029/2022JB024120.

Kusumoto, S., N. Geshi and A. Gudmundsson (2013). Aspect ratios and magma overpressures of non-feeder dikes observed in the Miyakejima volcano (Japan), and fracture toughness of its upper part, Geophys. Res. Lett., 40, 1065-1068, doi:10.1002/grl.50284.

Johnson, A. M. and D. D. Pollard (1973). Mechanisms of some laccolithic intrusions in the Henry Mountains, Utah, Part I: Field observations, Tectonophysics, 18, 261-309, doi:10.1016/0040-1951(73)90050-4.

Le Corvec, N., T. Menand and J. Lindsay (2013). Interaction of ascending magma with pre-existing crustal fractures in monogenetic basaltic volcanism: an experimental approach, J. Geophys. Res., Solid Earth, 118, 3, 968-984, doi:10.1002/jgrb.50142.

Maineri, C., M. Benvenuti, P. Costagliola, A. Dini et al. (2003). Sericitic alteration at the La Crocetta mine (Elba Island, Italy): interplay between magmatism, tectonics, and hydrothermal activity, Miner Deposita, 38, 67-86, doi:10.1007/s00126-002-0279-2.

Massa, G., G. Musumeci, F. Mazzarini and D. Pieruccioni (2017). Coexistence of contractional and extensional tectonics during the northern Apennines orogeny: the late Miocene out-of-sequence thrust in the Elba Island nappe stack, Geol. J., 52, 353-368, doi:10.1002/gj.2761.

Mazzarini, F. and G. Musumeci (2008). Hydrofracturing-related sill and dyke emplacement at shallow crustal levels: the Eastern Elba Dyke Complex, Italy, Geol. Soc. London, Spec. Publ., 302, 121-129, doi:10.1144/SP302.9.

Mazzarini, F., I. Isola, G. Ruggieri and C. Boschi (2010). Fluid circulation in the upper brittle crust: Thickness distribution, hydraulic transmissivity fluid inclusion and isotopic data of veins hosted in the Oligocene sandstones of the Macigno Formation in southern Tuscany, Italy, Tectonophysics, 493, 118-138, doi:10.1016/j.tecto.2010.07.012.

Mazzarini, F., G. Musumeci and A. R. Cruden (2011). Vein development during folding in the upper brittle crust: the case of tourmaline-rich veins of eastern Elba Island, northern Tyrrhenian Sea, Italy, J. Struct. Geol., 33, 1509-1522, doi:10.1016/j.jsg.2011.07.001.

Mazzarini, F., G. Ruggieri, I. Isola, C. Boschi et al. (2014). Fluid transfer and vein thickness distribution in high and low temperature hydrothermal systems at shallow crustal level in southern Tuscany (Italy), Ann. Geophys., 57, 3, S0326, doi:10.4401/ag-6263.

Mazzarini, F., L. Bracciali, G. Musumeci, J. R. Wijbrans et al. (2024). Coupled U–Pb and 40Ar/39Ar chronology of late-stage intrusions at Elba Island (Italy) supports late Miocene long-lived magma reservoirs in the Tyrrhenian upper crust, Terra Nova, 36, 258-265, doi:10.1111/ter.12706.

McCaffrey, K. and N. Petford (1997). Are granitic plutons scale invariant? J. Geol. Soc., London, 154, 1-4, doi:10.1144/gsjgs.154.1.0001.

Musumeci, G., F. Mazzarini, M. Tiepolo and G. Di Vincenzo (2011). U-Pb and 40Ar-39Ar geochronology of Paleozoic units in the northern Apennines: Determining protolith age and alpine evolution using the Calamita Schist and Ortano Porphyroid, Geol. J., 46, 288-310, doi:10.1002/gj.1266.

Musumeci, G. and L. Vaselli (2012). Neogene deformation and granite emplacement in the metamorphic units of northern Apennines (Italy): Insights from mylonitic marbles in the Porto Azzurro pluton contact aureole (Elba Island), Geosphere, 8, 2, 470-490, doi:10.1130/GES00665.1.

Musumeci, G., F. Mazzarini and A. R. Cruden (2015). The Zuccale Fault, Elba Island, Italy: a new perspective from fault architecture, Tectonics, 34, 1195-1218, doi:10.1002/2014TC003809.

Olson, J. E. (2003). Sublinear scaling of fracture aperture versus length: An exception or the rule?, J. Geophys. Res., Solid Earth, 108, 2413, doi:10.1029/2001JB000419.

Pagli, C., F. Mazzarini, D. Keir, E. Rivalta et al. (2015). Introduction: Anatomy of rifting: Tectonics and magmatism in continental rifts, oceanic spreading centers, and transforms, Geosphere, 11, 5, 1256-1261, doi:10.1130/GES01082.1.

Papeschi, S., G. Musumeci and F. Mazzarini (2017). Heterogeneous brittle-ductile deformation at shallow crustal levels under high thermal conditions: the case of a synkinematic contact aureole in the inner northern Apennines, southeastern Elba Island, Italy, Tectonophysics, 717, 547-564, doi:10.1016/j.tecto.2017.08.020.

Papeschi, S., G. Musumeci, H. J. Massonne, O. Bartoli et al. (2019). Partial melting and strain localization in metapelites at very low-pressure conditions: the northern Apennines magmatic arc on the Island of Elba, Italy, Lithos, 350, 105230, doi:10.1016/j.lithos.2019.105230.

Papeschi, S., E. Ryan, G. Musumeci, F. Mazzarini et al. (2021). Geology of the Northern Apennines nappe stack on eastern Elba (Italy): new insights on the Neogene orogenic evolution of the Northern Tyrrhenian Sea, J. Maps, 17, 2, 519-532, doi:10.1080/17445647.2021.1972854.

Papeschi, S., F. Mazzarini, G. Musumeci and A. R. Cruden (2022). Emplacement of a felsic dyke swarm during progressive heterogeneous deformation, Eastern Elba Dyke Complex (Island of Elba, Italy), J. Struct. Geol., 159, 104600, doi:10.1016/j.jsg.2022.104600.

Paterson, S. R. and O. T. Tobisch (1992). Rates of processes in magmatic arcs: implications for the timing and nature of pluton emplacement and wall rock deformation, J. Struct. Geol., 14, 3, 291-300, doi:10.1016/0191-8141(92)90087-D.

Pertusati, P. C., G. Raggi, C. A. Ricci, S. Duranti et al. (1993). Evoluzione post-collisionale dell'Elba centro-orientale, Mem. Soc. Geol. It., 49, 297-312.

Petford, N., A. R. Cruden, K. J. W. McCaffrey and J. L. Vigneresse (2000). Granite magma formation, transport and emplacement in the Earth's crust, Nature, 408, 669-673, doi:10.1038/35047000.

Petford, N. (2003). Rheology of granitic magmas during ascent and emplacement, Ann. Rev. Earth Planet Sci., 31, 399-427, doi:10.1146/annurev.earth.31.100901.141352.

Pfiffner, O. A. and J. G. Ramsay (1982). Constraints on Geological Strain Rates: Arguments From Finite Strain States of Naturally Deformed Rocks, J. Geophys. Res., Solid Earth, 87, B1, 311-321, doi:10.1029/JB087iB01p00311.

Pollard, D. D. and A. M. Johnson (1973). Mechanisms of some laccolithic intrusions in the Henry Mountains, Utah, Part II: Bending and failure of overburden and sill formation, Tectonophysics, 18, 311-354, doi:10.1016/0040-1951(73)90051-6.

Rocchi, S., D. S. Westerman, A. Dini, F. Innocenti et al. (2002). Two-stage growth of laccoliths at Elba Island, Italy, Geology, 30,983-30,986, doi:10.1130/0091-7613(2002)030<0983:TSGOLA>2.0.CO;2.

Rivalta, E., B. Taisne, A. P. Bunger and R. F. Katz (2015). A review of mechanical models of dike propagation: schools of thought, results and future directions, Tectonophysics, 638, 1-42, doi:10.1016/j.tecto.2014.10.003.

Sassier, C., P. H. Leloup, D. Rubatto, O. Galland et al. (2009). Direct measurement of strain rates in ductile shear zones: a new method based on syntectonic dikes, J. Geophys. Res., Solid Earth, 114, B1, B01406, doi:10.1029/2008JB005597.

Scholz, C. H. (2002). The Mechanics of Earthquakes and Faulting, 2 ed., Cambridge University Press, 471.

Schultz, R. A., R. Soliva, H. Fossen, C. H. Okubo et al. (2008a). Dependence of displacement-length scaling relations for fractures and deformation bands on the volumetric changes across them, J. Struct. Geol., 30, 1405-1411, doi:10.1016/j.jsg.2008.08.001.

Schultz, R. A., D. Mège and H. Diot (2008b). Emplacement conditions of igneous dikes in Ethiopian Traps, J. Volcanol. Geotherm. Res., 178, 683-692, doi:10.1016/j.jvolgeores.2008.08.012.

Siniscalchi, A., I. Diaferia, M. P. Liuni, M. Loddo et al. (2008). Integrated geophysical approach for imaging the Porto Azzurro (Elba, Italy) plutons and the associated structures, in Oslo, Proceedings 33rd International Geological Congress, 6-14 August 2008.

Smith, R. J. (2009). Use and misuse of the reduced major axis for line-fitting, Am. J. Phys. Anthropol., 140, 476-486, doi:10.1002/ajpa.21090.

Spiess, R., A. Langone, A. Caggianelli, F. M. Stuart et al. (2021). Unveiling ductile deformation during fast exhumation of a granitic pluton in a transfer zone, J. Struct. Geol., 147, 104326, doi:10.1016/j.jsg.2021.104326.

Thomson, K. and D. Hutton (2004). Geometry and growth of sill complexes: insights using 3D seismic from the North Rockall Trough, Bull. Volc., 66, 364-375, doi:10.1007⁄s00445-003-0320-z.

***CORRESPONDING AUTHOR: Francesco MAZZARINI**,
Istituto Nazionale di Geofisica e Vulcanologia, Pisa
Via Cesare Battisti 53, 56125, Pisa Italy
e-mail: francesco.mazzarini@ingv.it